Subcircuit Modeling of Magnetic Cores with Hysteresis in PSpice

A methodology to develop subcircuit models of magnetic cores with hysteresis using analog behavioral modeling (ABM) in PSpice is presented. A subcircuit equivalent to the Jiles–Atherton model is developed to model the static ferromagnetic hysteresis. The Hammerstein configuration, which includes a nonlinear static block followed by a linear dynamic block, is further employed to capture the rate dependencies. The nonlinear static block is realized by the Jiles–Atherton model, and linear dynamic block by a low-pass filter. Interface subcircuits are provided to couple the voltage induced by the magnetic flux to the winding model of an inductor or a transformer. The hysteresis-related waveforms predicted by the developed inductor and transformer subcircuit models have been verified experimentally.

I. INTRODUCTION

Computer simulation is now an integral part of a design cycle for an aeronautic power converter. In order to provide realistic results, the simulator needs to make available to the users reliable models for the converter components. Such a model is presented here for the magnetic cores ubiquitously present in aerospace power supplies. Although the model is portable to most commercial circuit simulators, PSpice [1] (evaluation version) is employed to exemplify the specifics.

As other modern simulators, PSpice offers analog behavioral modeling (ABM) capability. ABM can solve general mathematical problems by translating the governing equations into an electrical circuit with controlled voltage sources and controlled current sources [2]. Thus, the availability of ABM in PSpice has made easier the implementation of those new or developing models that are not sufficiently mature to be coded directly into PSpice.

ABM had been applied in [3] to model the hysteresis loop. Several look-up-table controlled sources were used to perform piecewise-linear approximations of different regions of the B-H characteristics, and a Schmidt trigger circuit was employed to generate the hysteresis. The modeling approach using several look-up tables is not convenient, since all the table contents have to be changed if the simulated core material is changed. Therefore, a plethora of experimental data needs to be measured before building a components library. On the contrary, only several material parameters need to be extracted if physics-based models [4, 5] or behavioral models [6, 7] are used.

The initial motivation of the work was to develop ABM-based subcircuits for modeling of hysteresis phenomena using physics-based models. In a previous work [8], a modified Preisach model [10] was used to realize the nonlinear static block in the Hammerstein configuration, and the model variables that need to be memorized were implemented as analog states in the SABER circuit simulator [9]. The ABM in PSpice, however, does not provide an easy way to model the state behavior. Thus, the Jiles–Atherton model [4, 5] is employed herein instead of the Preisach model. Although the Jiles–Atherton model has been implemented in PSpice to model magnetic cores, it is difficult to modify the source code for the inclusion of other, e.g., dynamic, effects.

The first contribution of the work reported here is to modify the Jiles–Atherton model to capture the dynamic hysteresis phenomena in PSpice. The second contribution is a methodology to develop subcircuit models of magnetic components with hysteresis using ABM in PSpice. A subcircuit equivalent to the Jiles–Atherton model is developed to model the static ferromagnetic hysteresis. A linear dynamic block (e.g., a second-order low-pass filter) then follows the static hysteresis block to capture the rate dependency in the core, as suggested by Hammerstein [6, 7]. Developed in the "evaluation version" of PSpice, the subcircuits are expected to be portable to those simulators that support ABM-like features. The core equivalent subcircuit can be incorporated in the finite-element simulation described in [11] to simulate coupled field and circuit phenomena. The voltage induced by the magnetic flux is coupled to the windings via interface subcircuits. Magnetic component windings are not considered herein, but could be incorporated in future work using, e.g., the approach described in [18].

Following this section, the mathematical background of the core and winding models is reviewed in Section II. The ABM-based subcircuit models are described in Section III. Model implementation and parameter extraction are discussed in Section IV. The developed subcircuit models are verified experimentally in Section V. Section VI concludes the paper.

II. MATHEMATICAL BACKGROUND

The governing equations for the Jiles–Atherton hysteresis model, and for an inductor and a transformer are reviewed in this section. The Hammerstein model is also reviewed.

Manusript received October 24, 2001; revised July 22, 2002.

IEEE Log No. T-AES/38/4/06566.

Refereeing of this contribution was handled by W. M. Polivka.

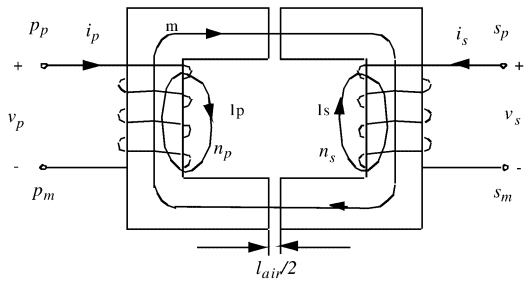

Fig. 1. Two-winding transformer.

A. Governing Equations of the Jiles–Atherton Model

The governing equations of the Jiles–Atherton model are summarized as follows:

$$\frac{dM_{irr}}{dH} = \frac{M_{an} - M_{irr}}{k\delta - \alpha(M_{an} - M_{irr})} \tag{1}$$

$$M_{an} = M_s \left[\coth\left(\frac{H + \alpha M}{a}\right) - \frac{a}{H + \alpha M}\right] \tag{2}$$

$$M_{rev} = c(M_{an} - M_{irr}) \tag{3}$$

$$M = M_{irr} + M_{rev} \tag{4}$$

where M is the magnetization; M_{irr} the irreversible magnetization; M_{rev} the reversible magnetization; M_{an} the anhysteretic magnetization; and H the magnetic field intensity. The five model parameters are M_s, the saturation magnetization in A/m; α, the experimentally obtained mean field parameter (dimensionless); a, the shape parameter in A/m; k, the domain wall pinning constant in A/m; and c, the domain wall flexing constant. Note that k gives a measure of the width of the hysteresis loop, and there is no hysteresis if $k = 0$. The directional parameter δ is $+1$ for $dH/dt > 0$, and -1 for $dH/dt < 0$. To calculate the magnetic flux density B from M and H, the following constitutive law of the magnetic material property is used

$$B = \mu_0(M + H) \tag{5}$$

where $\mu_0 = 4\pi \times 10^{-7}$ (H/m) is the permeability of free space. More details about the Jiles–Atherton model can be found in [4, 5].

B. Governing Equations for a Transformer

For the two-winding transformer shown in Fig. 1, the total flux enclosed by the primary winding is

$$\Phi_{np} = \Phi_m + \Phi_{lp} \tag{6}$$

and the total flux enclosed by the secondary winding is

$$\Phi_{ns} = \Phi_m + \Phi_{ls} \tag{7}$$

where Φ_m is the flux inside the magnetic core; Φ_{lp} and Φ_{ls} are the primary and secondary leakage fluxes, respectively. Using Faraday's law, the voltages v_P induced in the primary winding, and v_S in the secondary winding are given by

$$v_P = n_p\frac{d\Phi_{np}}{dt} = n_p\frac{d\Phi_m}{dt} + n_p\frac{d\Phi_{lp}}{dt} = n_P\frac{d(BS_C)}{dt} + L_P\frac{di_P}{dt} \tag{8}$$

$$v_s = n_s\frac{d\Phi_{ns}}{dt} = n_s\frac{d\Phi_m}{dt} + n_s\frac{d\Phi_{ls}}{dt} = n_s\frac{d(BS_C)}{dt} + L_s\frac{di_s}{dt} \tag{9}$$

where S_c is the cross-sectional area; i_P and i_S are the primary and secondary currents, respectively; n_p and n_s are the numbers of primary and secondary turns, respectively; and L_P and L_S are the primary and secondary leakage inductances, respectively. Note that the relations: $\Phi_m = BS_c$, $n_p\Phi_{lp} = L_p i_p$ and $n_s\Phi_{ls} = L_s i_s$ have been applied in the above two equations.

Using Ampere's law, we can write

$$H \cdot l_m + H_{air} \cdot l_{air} = n_P \cdot i_P + n_S \cdot i_S \tag{10}$$

where l_m is the magnetic mean path; l_{air} the air gap length; and $H_{air} = B/\mu_0$ is the field intensity in the air. Thus, the magnetic field intensity H can be expressed as

$$H = \frac{n_p \cdot i_p + n_s \cdot i_s - \dfrac{B}{\mu_0} \cdot l_{air}}{l_m}. \tag{11}$$

The subcircuit model of a transformer with hysteresis is built from (1)–(5), (8), (9), (11), and a linear dynamic block realized by a low-pass filter in the Hammerstein configuration.

Here, the coupling among H, B, terminal currents (i_P, i_S), and terminal voltages (v_P, v_S) can be illustrated using (1)–(5), (8), (9), and (11). As shown in (11), H is mainly determined from the terminal currents (neglecting the effect of air gap). From any hysteresis model, e.g., (1)–(5) of the Jiles–Atherton model, B can be found from H. The terminal voltages are then mainly determined from B (neglecting the effect of leakage inductances), as shown in (8) and (9). Finally, the terminal currents (i_P, i_S) can be obtained from the terminal voltages (v_P, v_S) through the global circuit containing the transformer. Thus, H, B, terminal currents, and terminal voltages are highly coupled in the transformer subcircuit model. To avoid convergence problems in PSpice simulation of the subcircuit models, the limit at any repeating point in transient analysis, i.e., parameter ITL4 inside Analysis/setup/option on the Schematics window, sometimes has to be increased from the default value 10 to about 100–1000, and the Step Ceiling inside Analysis/setup/transient has to be well controlled.

C. Governing Equations for an Inductor

Similarly for an inductor, the voltage v_L induced in the winding by the total flux Φ_n, and the magnetic

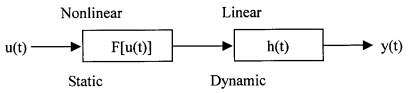

Fig. 2. Configuration of Hammerstein model.

field intensity H are given by

$$v_L = n\frac{d\Phi_n}{dt} = n\frac{d(BS_C)}{dt} + L_l\frac{di_L}{dt} \tag{12}$$

$$H = \frac{n \cdot i_L - \dfrac{B}{\mu_0} \cdot l_{air}}{l_m} \tag{13}$$

where i_L is the current flowing through the inductor; L_l the leakage inductance; and n the number of winding turns. The subcircuit model of an inductor with hysteresis is built from (1)–(5), (12), (13), and a linear dynamic block realized by a low-pass filter in the Hammerstein configuration.

D. The Hammerstein Model

As shown in Fig. 2, a Hammerstein model consists of a nonlinear static block followed by a linear dynamic block. The Hammerstein model represents a realization of the Hammerstein operator

$$H[u(t)] = \int_0^t h(t,\tau)F[\tau,u(\tau)]d\tau \tag{14}$$

which is simplified to

$$H[u(t)] = \int_0^t h(t-\tau)F[u(\tau)]d\tau \tag{15}$$

for a nonlinear time-invariant system [6, 7]. The Hammerstein configuration is applied herein to capture the rate-dependent effects of hysteresis phenomena. In the developed ABM-based dynamic hysteresis circuit, the Jiles–Atherton model is used to realize the nonlinear static block, and a low-pass filter is used to realize the linear dynamic block.

III. DEVELOPMENT OF EQUIVALENT SUBCIRCUITS

The first step to build magnetic subcircuit models is to develop subcircuits equivalent to the Jiles–Atherton model for static ferromagnetic hysteresis, and linear filter subcircuits to capture the rate-dependent hysteresis phenomena. Interface subcircuits equivalent to the governing equations of an inductor or a transformer are also developed, and integrated with the developed dynamic hysteresis circuit to build magnetic subcircuit models. These ABM-based subcircuits are discussed in this section.

A. Subcircuits Modeling Static Hysteresis

An ABM-based subcircuit equivalent to the Jiles–Atherton model is shown in Fig. 3, where controlled voltage sources (EVALUE, E) and a

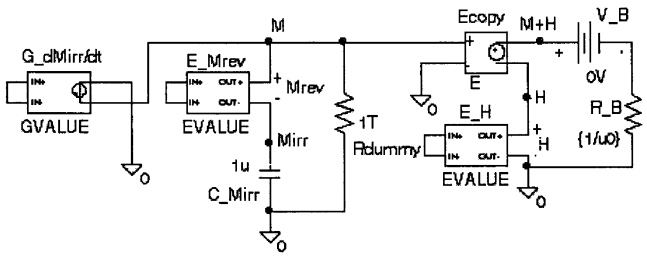

Fig. 3. ABM-based subcircuit for modeling of static hysteresis based on Jiles–Atherton model.

controlled current source (GVALUE), as well as one capacitor and two resistors are used to simultaneously realize (1)–(5). In the circuit, the irreversible magnetization M_{irr}, the magnetization M, the magnetic field intensity H, and $M + H$ are chosen as node voltages. The resistor R_{dummy} is used to avoid floating nodes in the circuit, and R_B is used to generate B from $M + H$.

From (1) and (3),

$$\frac{dM_{irr}}{dt} = \frac{\dfrac{M_{rev}}{c}}{k\delta - \alpha \cdot \dfrac{M_{rev}}{c}} \cdot \frac{dH}{dt} \tag{16}$$

which is modeled by the controlled current source, G_dM$_{\text{irr}}$/dt (GVALUE), in Fig. 3. From the current/voltage relation of a capacitor, the current flowing in the loop containing G_dM$_{\text{irr}}$/dt, E_M$_{\text{rev}}$ and C_M_{irr} can be expressed as

$$i = C\_M_{irr}\frac{dM_{irr}}{dt} = 1u \cdot \frac{dM_{irr}}{dt} \tag{17}$$

where M_{irr} is the voltage across the capacitor C_M_{irr}. In the circuit, $C\_M_{irr} = 1uF$ is chosen to avoid unreasonable currents since voltages and currents in PSpice are limited to $+/-1e10$ and derivatives in PSpice are limited to 1e14. Expressing the current in G_dM$_{\text{irr}}$/dt (GVALUE) as

$$i = 1u \cdot \frac{\dfrac{M_{rev}}{c}}{k\delta - \alpha \cdot \dfrac{M_{rev}}{c}} \cdot \frac{dH}{dt} \tag{18}$$

(16) is satisfied, and (1) in the Jiles–Atherton model is thus included in the circuit.

Both (2) and (3) are modeled together by the controlled voltage source, E_M$_{\text{rev}}$ (EVALUE), by placing the expression of M_{an} in (2) into (3), and (4) is automatically satisfied in the circuit ($v(M) = v(M_{irr}) + v(M_{rev})$). Either (13) for an inductor or (11) for a transformer is put into the controlled voltage source, E_H (EVALUE), to model H. Note that both E_copy (E) and E_H (EVALUE) make $M + H$ as a node voltage. Choosing R_B= $1/\mu_0$, (5) is thus satisfied; and B is equal to the current flowing through the dummy voltage source, V_B. Plotting I(V_B) versus v(H) in PSpice would generate the static B-H hysteresis loop.

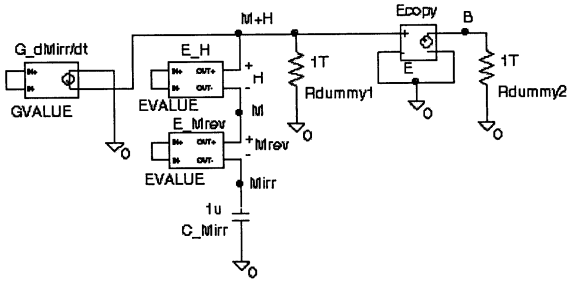

Fig. 4. Alternative ABM-based subcircuit for modeling of static hysteresis based on Jiles–Atherton model.

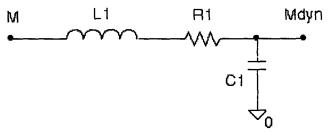

Fig. 5. RLC circuit representing second-order low-pass filter.

An alternative ABM-based subcircuit equivalent to the Jiles–Atherton model is shown in Fig. 4, where the location of E_H (EVALUE) is different from that in Fig. 3. In the circuit, both R_{dummy1} and R_{dummy2} are dummy resistors used to avoid floating nodes, and B can be directly obtained as a node voltage by setting the gain of Ecopy (E) to μ_0. Plotting v(B) versus v(M+H)-v(M) in PSpice would generate the static B-H hysteresis loop. Both circuits in Figs. 3 and 4 have been implemented and verified in PSpice. The simulation speed and resulting hysteresis curves using circuits in Figs. 3 or 4 are almost the same.

B. Subcircuit Modeling Rate-Dependent Hysteresis

The second-order low-pass filter shown in Fig. 5 is used to realize the linear dynamic block in Fig. 2. For this circuit, the transfer function is written as

$$\frac{M_{dyn}(s)}{M(s)} = \frac{1}{L_1C_1s^2 + R_1C_1s + 1} \tag{19}$$

where M is the static magnetization, and M_{dyn} the dynamic magnetization. In the work, $C_1 = 1uF$ is chosen, and L_1 and R_1 are the model parameters to be extracted. It is noted that (19) is similar to the dynamic model discussed in [12]. Circuit analysis of Fig. 5 gives

$$L_1C_1\frac{d^2M_{dyn}(t)}{dt^2} + R_1C_1\frac{dM_{dyn}(t)}{dt} + M_{dyn}(t) = M(t). \tag{20}$$

The model in [12] can be written in a similar form as

$$\frac{1}{\omega_n^2}\frac{d^2M_{dyn}(t)}{dt^2} + \frac{2\lambda}{\omega_n^2}\frac{dM_{dyn}(t)}{dt} + M_{dyn}(t) = M(t). \tag{21}$$

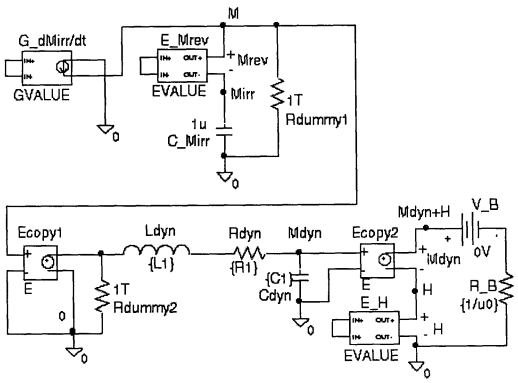

Fig. 6. Hammerstein-based circuit for modeling of dynamic hysteresis phenomena.

Comparing the above two equations, we can write

$$L_1C_1 = \frac{1}{\omega_n^2}; \qquad R_1C_1 = \frac{2\lambda}{\omega_n^2}. \tag{22}$$

Thus, let $C_1 = 1uF$, L_1 is related to the natural frequency ω_n, and R_1 to the damping constant λ of the material. Note that other filter types or orders could be used to realize the linear dynamic block, if more accuracy is desired. Thus, the model in [12] is only a special case of the presented model, with the dynamic block realized by a second-order low-pass filter.

Insertion of the subcircuit in Fig. 5 into the subcircuit in Fig. 3 results in Fig. 6, which models the dynamic hysteresis in the core. Note that M in (5) has been replaced by the dynamic magnetization M_{dyn}. As can be seen, Fig. 5 is easier to integrate with Fig. 3 than Fig. 4.

C. Interface Subcircuits for an Inductor or a Transformer

The interface subcircuit that couples the flux-induced voltage into an inductor winding is shown in Fig. 7(a). A dummy voltage source, V_IL, is used to sense the inductor current for calculating H in the previously developed hysteresis circuits. Equation (12) is modeled by the controlled voltage source, E_VL (EVALUE).

The interface subcircuit that couples the flux-induced voltage into the transformer windings is shown in Fig. 7(b). Dummy voltage sources, V_IP and V_IS, are used to sense the primary and secondary currents, respectively, and (8) is modeled by E_VP, and (9) by E_VS.

IV. MODEL IMPLEMENTATION AND PARAMETER EXTRACTION

A. Model Implementation

The subcircuits in Figs. 6 and 7 can be integrated to build inductor or transformer subcircuit models

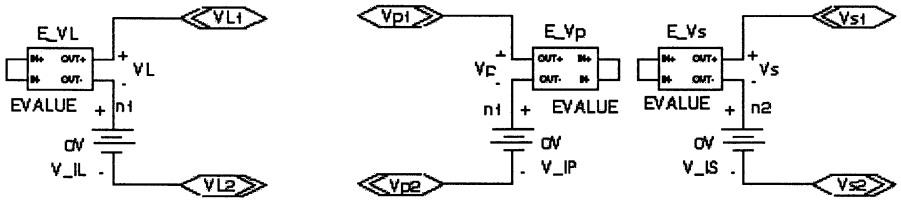

Fig. 7. Interface subcircuits to couple the flux-induced voltages into the windings of (a) an inductor and (b) a transformer.

TABLE I
The .SUBCKT Statements for Transformer Subcircuit Model

```
.SUBCKT T_dyn Vp1 Vp2 Vs1 Vs2 PARAMS: Ms=3.8E5 a=27 c=0.33 k=25 alpha=1E-4
+Lm=0.0295 Sc=1.28E-5 np=18 ns=18 lair=0 Lp=0 Ls=0 L1=15n R1=0.12 C1=1u
.PARAM u0={4*3.14159*1E-7}
E_Vp Vp1 n1 VALUE={np*DDT(I(V_B))*Sc+Lp*DDT(I(V_Ip))}
V_Ip n1 Vp2 0V
E_Vs Vs1 n2 VALUE={ns*DDT(I(V_B))*Sc+Ls*DDT(I(V_Is))}
V_Is n2 Vs2 0V
E_Mrev M Mirr VALUE={c*(Ms*(1/tanh((v(H)+alpha*v(M))/a)-a/(v(H)+alpha*v(M))) + -v(Mirr))}
C_Mirr Mirr 0 1u
Rdummy1 M 0 1T
G_dMirr/dt 0 M VALUE={1u*DDT(v(H))/(k*SGN(DDT(v(H)))*c/(v(M)-v(Mirr))-alpha)}
Ecopy1 n3 0 M 0 1.0
Ldyn n3 n4 {L1}
Rdyn n4 Mdyn {R1}
Cdyn Mdyn 0 {C1}
Rdummy2 n3 0 1T
Ecopy2 Mdyn+H H Mdyn 0 1.0
E_H H 0 VALUE={(np*I(V_Ip)+ns*I(V_Is)-v(Mdyn+H)*lair)/Lm}
V_B Mdyn+H n5 0V
R_B n5 0 {1/u0}
.ENDS T_dyn
```

with dynamic hysteresis. The .SUBCKT statements for a transformer subcircuit are shown in Table I to illustrate model implementation in PSpice. To create a subcircuit model, the .SUBCKT statements, as those in Table I, have to be written by a text editor and saved in a file with .lib extension. The next step is to add a symbol for the created subcircuit model by selecting [Edit Library] from the [File] menu on the Schematics window. After entering part definition and attributes and drawing the graphic symbol, the result can be saved to a file with .slb extension. To apply the created subcircuit models in simulation, the created *.slb file is added to the simulator by selecting [Editor Configuration] from the [Options] menu, and the created *.lib file by selecting [Library and Include Files] from the [Analysis] menu. More details about the model implementation can be found in the PSpice user's manual [1].

As shown in Table I, the symbol DDT represents d/dt, and SGN denotes the sign function, i.e., $\mathrm{SGN}(x) = 1$ for $x > 0$, and $\mathrm{SGN}(x) = -1$ for $x < 0$. The δ in (1) is thus modeled using the SGN function. Also note that the $\coth(x)$ function has to be replaced by $1/\tanh(x)$ in PSpice.

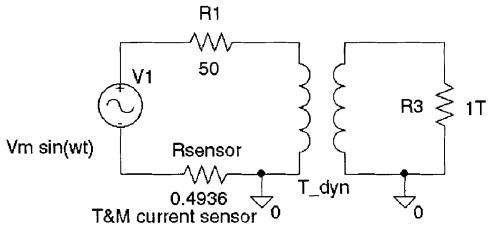

Fig. 8. Simulation circuit for verification of developed transformer subcircuit model.

B. Parameter Extraction

As described in [5], the five parameters of the Jiles–Atherton model can be calculated from experimental measurements of coercivity, remanence, saturation magnetization, initial anhysteretic susceptibility, initial normal susceptibility, and the maximum differential susceptibility. This experimental approach for parameter extraction, however, is somewhat difficult to employ for common users of PSpice. Based on the fact that each of the five parameters has some effects on the shape of the hysteresis loop, a searching procedure using a multiple-plot technique in PSpice was described in [13]. This parameter extraction procedure may be

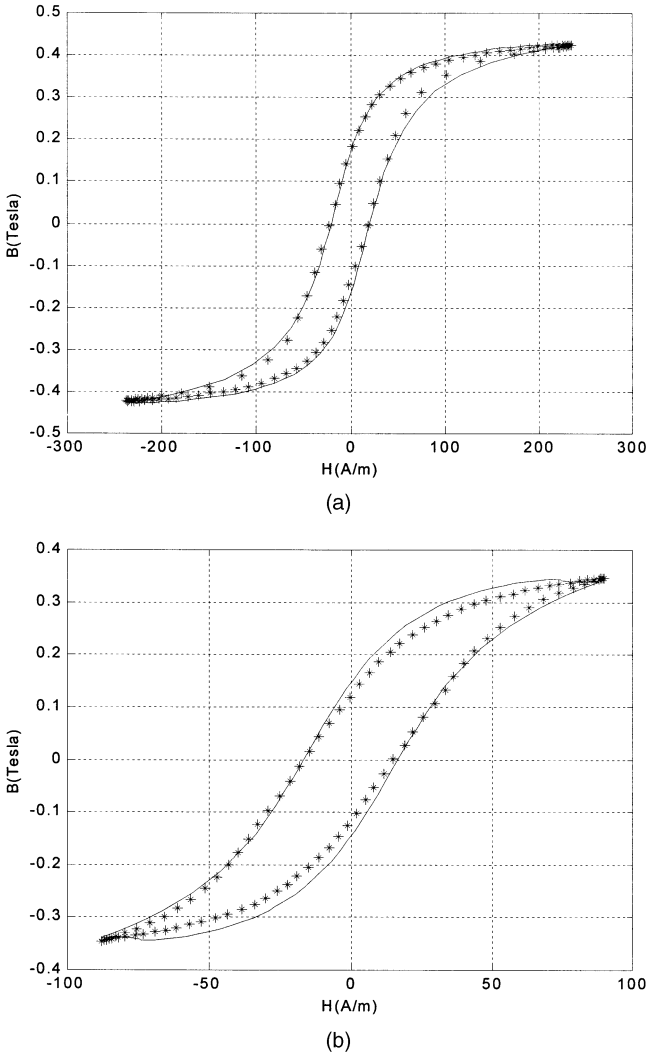

Fig. 9. Comparison of simulated and measured hysteresis curves at (a) $V_m = 20$ V, and (b) $V_m = 10$ V and $f = 10$ kHz. Solid lines are simulated curves. *** measured curves.

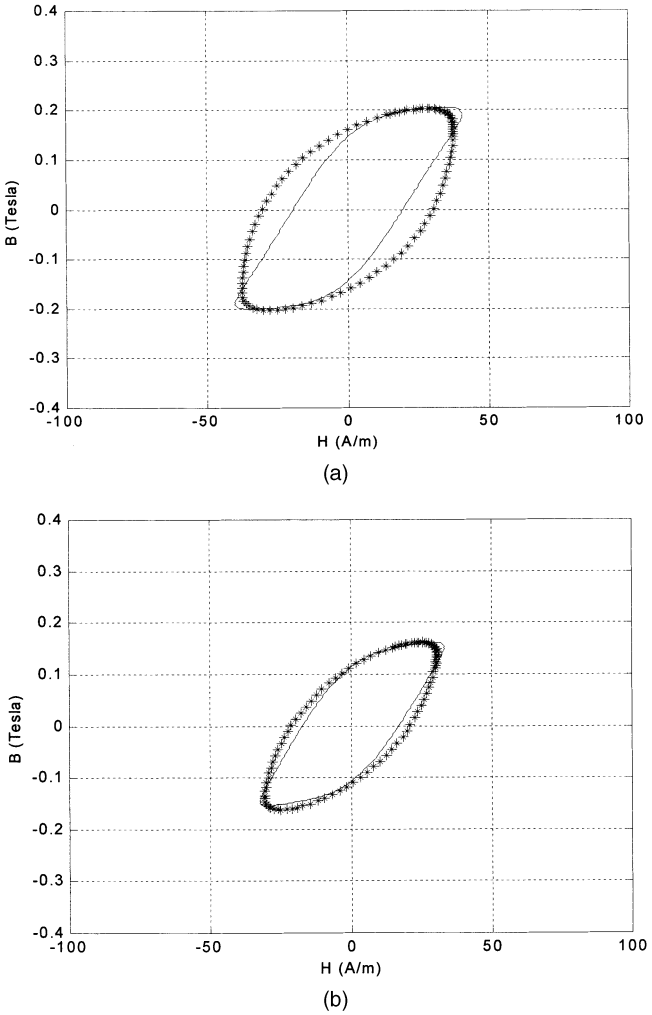

Fig. 10. Comparison of simulated and measured hysteresis curves at (a) $V_m = 90$ V, and (b) $V_m = 70$ V and $f = 300$ kHz. Solid lines are simulated curves. *** measured curves.

easier to use for common users of PSpice. Numerical techniques such as simulating annealing, genetic algorithm, or a combination of both methods were also discussed in [14, 15] for extraction of the Jiles–Atherton model parameters. In this work, the multiple-plot technique in PSpice is used to extract the five Jiles–Atherton model parameters.

The magnetic core material used for verification of the magnetic subcircuit models is the 3C85 ferrite [16]. From the measured curves and the multiple-plot technique, the following Jiles–Atherton model parameters were found to give the best fit between simulation and measurements: $M_S = 3.8 \times 10^5$ A/m, $a = 27$ A/m, $k = 25$ A/m, $\alpha = 1 \times 10^{-4}$, and $c = 0.33$. These values are consistent with those reported in [17]: $M_S = 3.8 \sim 3.98 \times 10^5$ A/m, $a = 27$ A/m, $k = 16 \sim 30$ A/m, $\alpha = 5 \times 10^{-5}$, and $c = 0.55$.

With $C_1 = 1uF$, L_1 and R_1 in the low-pass filter can be extracted from the least-squares estimation method discussed in [8]. The results are $L_1 = 15$ nH and $R_1 = 0.12\ \Omega$. The extracted model parameters and other geometry parameters for a transformer subcircuit model are shown in Table I.

V. MODEL VERIFICATION

The core-loss measurement setup to obtain the *BH* data had been discussed in [8]. A simulation circuit corresponding to the measurement setup is shown in Fig. 8, which is used to generate simulation data for verification of the developed transformer subcircuit model, using the parameters extracted in the previous section. The frequency range employed was 10–300 kHz due to equipment limitations. The tested core part number was Ferroxcube/Philips-768T188 with outer diameter (OD) = 12.7 mm, inner diameter (ID) = 7.14 mm, thickness = 4.78 mm, $l_m = 29.5$ mm, and $S_C = 1.28 \times 10^{-5}$ m^2. A primary winding and secondary winding were wound in a bifilar fashion on the core, both having 18 AWG #28 turns.

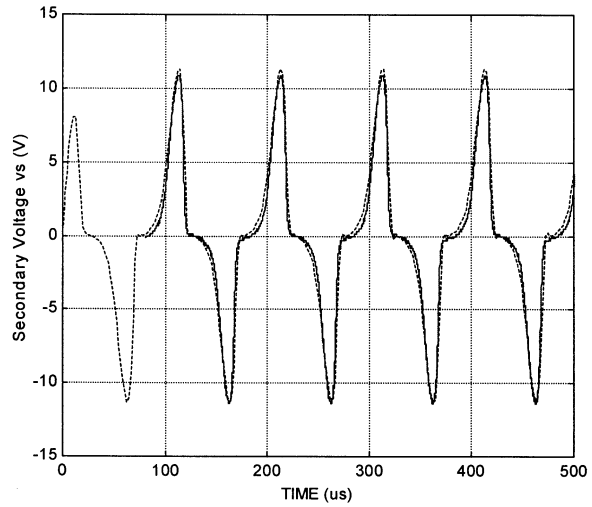

(a)

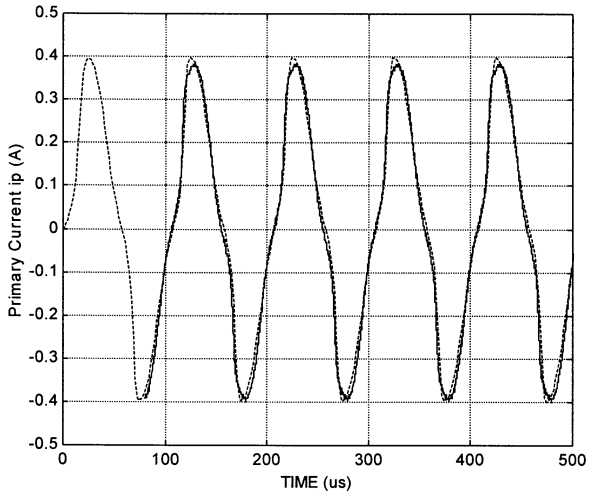

(b)

Fig. 11. Comparison of simulated and measured (a) secondary voltages, and (b) primary currents from the circuit shown in Fig. 8 at $V_m = 20$ V and $f = 10$ kHz. Dashed lines are simulated curves. Solid lines are measured curves.

The simulated curves were extracted from the PSpice simulation data, and were replotted with measured curves for comparison. The simulated and measured hysteresis loops at $f = 10$ kHz are shown in Fig. 9, and those at $f = 300$ kHz are shown in Fig. 10. The plots show the widening of the BH loops as frequency increased. The simulated secondary voltage v_S and primary current i_P at $V_m = 20$ V and $f = 10$ kHz are compared with the measured waveforms in Fig. 11. Fig. 12 shows the plot of initial permeability versus frequency obtained from an ac simulation of the circuit shown in Fig. 8. The total job time in PSpice for the ac simulation is 0.64 s. Overall, the agreement between theory and measurements is better at lower frequencies. Perhaps the model configuration in Fig. 2 or the dynamic structure in Fig. 5 could be modified in future work to better capture high-frequency hysteretic phenomena.

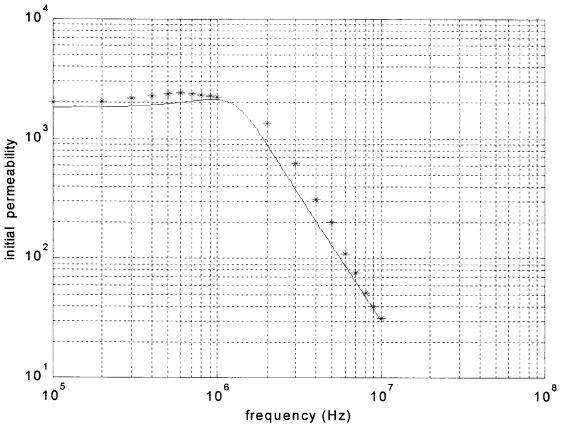

(a)

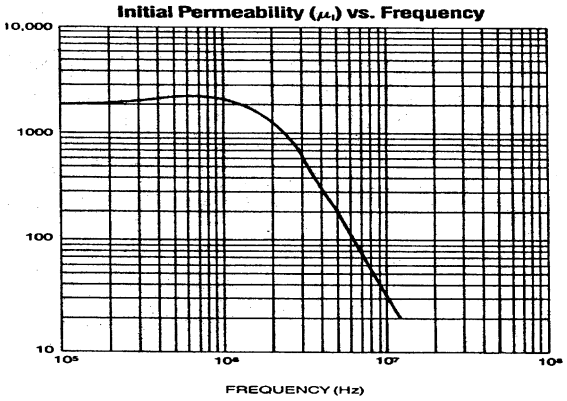

(b)

Fig. 12. (a) The plot of initial permeability versus frequency. Solid line is simulated curve. *** is measured data extracted from (b) for comparison. (b) Measured curve of initial permeability versus frequency for the 3C85 ferrite material copied from [16].

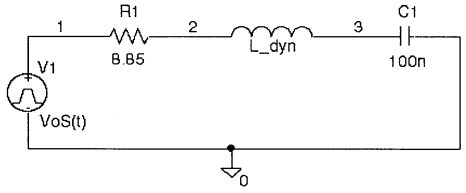

Fig. 13. Simulation circuit for verification of developed inductor subcircuit model.

To verify the developed inductor subcircuit model, the circuit shown in Fig. 13 is simulated to duplicate the $i - v_c$ phase-plane diagrams presented in [17]. As in [17], the best-fit Jiles–Atherton model parameters for the 3C85 ferrite in the PSpice simulation are: $M_S = 2.75 \times 10^5$ A/m, $a = 14.1$ A/m, k=17.8 A/m, $\alpha = 5 \times 10^{-5}$, and $c = 0.55$, and the other model parameters are: $l_m = 75.4$ mm, $S_C = 4.54 \times 10^{-5}$ m^2, $l_{air} = 0$, and $n = 230$ turns. The exciting voltage in Fig. 13 is a square wave with amplitude denoted by V_o and $f = 1.5$ kHz. Figs. 14(a) and 15(a) show the simulated $i - v_c$ phase-plane diagrams at $V_o = 13.5$ V (asymmetric period-2) and 20 V (symmetric period-3), respectively. The total job time in PSpice to obtain

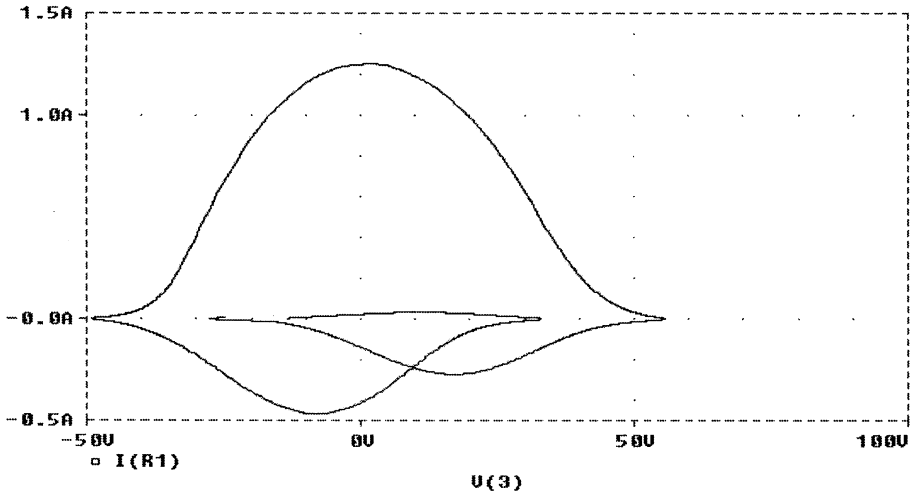

(a)

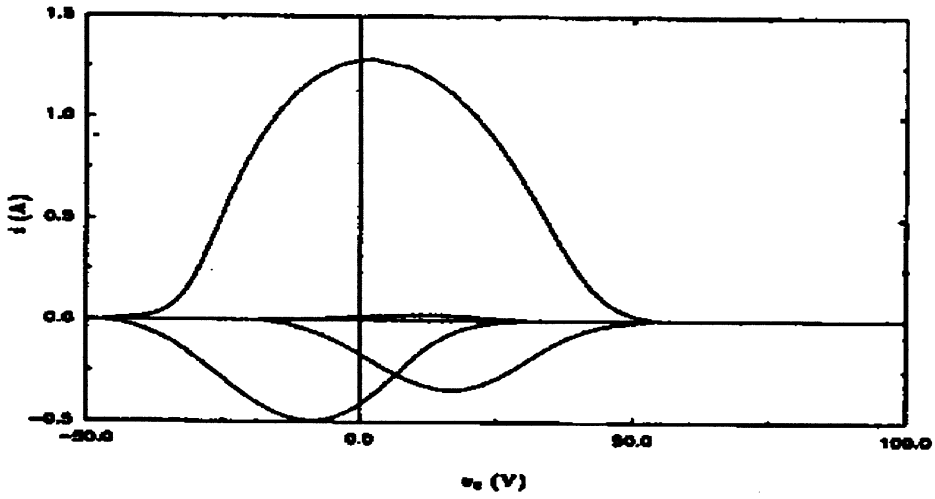

(b)

Fig. 14. (a) Simulated i–v_c phase-plane diagram obtained for $V_o = 13.5$ V (asymmetric period-2) from circuit shown in Fig. 13. (b) i–v_c phase-plane diagram at the same simulation conditions, which is copied from [17, Fig. 7(c)].

Fig. 15(a) is 7.24 s, under the following simulation conditions: final time = 1.666 ms, Step ceiling = 110 ns, ITL4 = 4000, and RELTOL = 0.001. It can be seen that Figs. 14(a) and 15(a) are almost identical to Figs. 14(b) and 15(b) which are copied from Figs. 7(c) and 7(e) in [17], respectively. Note that the simulation plots copied from [17] have been verified experimentally.

VI. CONCLUSION

A methodology has been presented to develop subcircuit models of magnetic cores with hysteresis using ABM in PSpice. The Hammerstein configuration, which includes a nonlinear static block followed by a linear dynamic block, has been applied to build an ABM-based hysteresis circuit to model the rate-dependent hysteresis phenomena. The Jiles–Atherton model is used to realize the nonlinear static block, and a second-order low-pass filter is used to realize the linear dynamic block, which takes into account the rate-dependent effects of hysteresis phenomena. The developed magnetic subcircuit models have been implemented in PSpice, and verified experimentally. A future work is to incorporate the ABM-based hysteresis circuit into finite-element formulation to build field-based subcircuits for modeling of magnetic components with dynamic hysteresis in PSpice. Expressing the model parameters as piecewise-linear functions of temperature could incorporate temperature dependencies. To improve the accuracy of high-frequency hysteresis curves, other model configurations and dynamic functions should be explored.

JIA-TZER HSU
Dept. of Information Engineering
Hung-Kuang Institute of Technology
Shalu, Taichung 433
Taiwan, R.O.C.

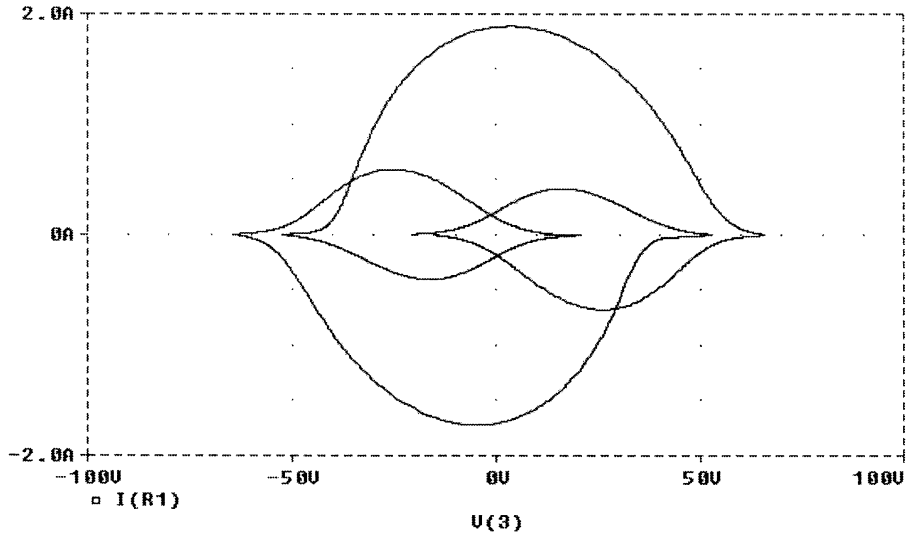

(a)

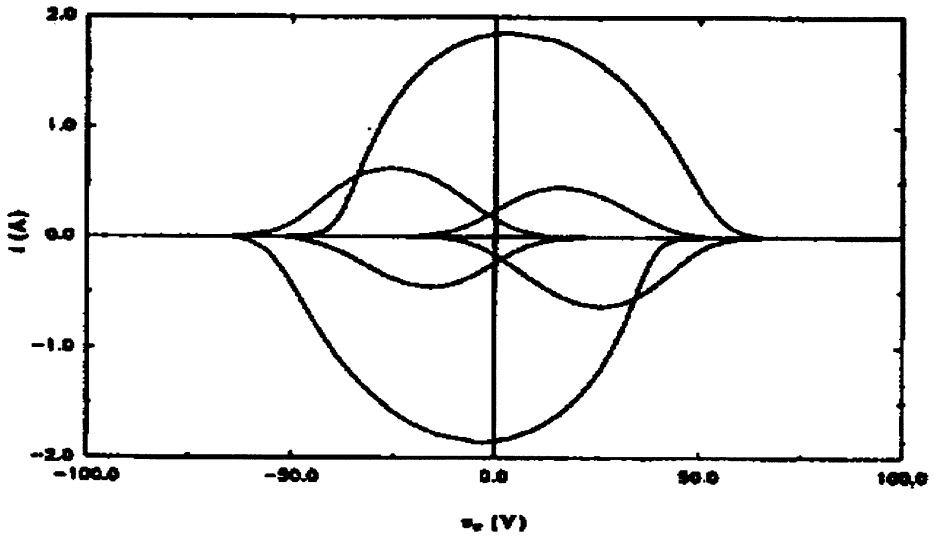

(b)

Fig. 15. (a) Simulated i–v_c phase-plane diagrams obtained for $V_o = 20$ V (symmetric period-3) from the circuit shown in Fig. 13. (b) i–v_c phase-plane diagram at the same simulation conditions, which is copied from [17, Fig. 7(e)].

KHAI D. T. NGO
Dept. of Electrical & Computer Engineering
University of Florida
557 Engineering Bldg.
PO Box 116130
Gainesville, FL 32611

REFERENCES

[1] *PSpice User's Manual* (1996)
MicroSim Corp., Irvine, CA, Apr. 1996.

[2] Cotorogea, M. (1998)
Implementation of mathematical models of power devices for circuit simulation in PSpice.
IEEE 6th Workshop on Computer in Power Electronics, 1998, 17–22.

[3] Maxim, A., Andreu, D., and Boucher, J. (1999)
A new Spice behavioral macromodeling method of magnetic components including the self-heating process.
IEEE Power Electronics Specialists Conference Record, vol. 2, 1999, 735–740.

[4] Jiles, D. C., and Atherton, D. L. (1986)
Theory of ferromagnetic hysteresis.
Journal of Magnetism and Magnetic Materials, **61** (1986), 48–60.

[5] Jiles, D. C., Thoelke, J. B., and Devine, M. K. (1992)
Numerical determination of hysteresis parameters for the modeling of magnetic properties using the theory of ferromagnetic hysteresis.
IEEE Transactions on Magnetics, **28**, 1 (Jan. 1992), 27–35.

[6] Billings, S. A. (1980)
Identification of nonlinear systems—A survey.
Proceedings of the Institution of Electronics Engineering, **127**, pt. D, 6 (1980), 272–285.

[7] Eskinat, E., Johnson, S. H., and Luyben, W. L. (1991)
Use of Hammerstein models in identification of nonlinear systems.
AIChE Journal, **37**, 2 (1991), 255–268.

[8] Hsu, J. T., and Ngo, K. D. T. (1997)
A Hammerstein-based dynamic model for hysteresis phenomenon.
IEEE Transactions on Power Electronics, **12**, 3 (May 1997), 406–413.

[9] *SABER User's Guide* (1992)
Release 3.4b, Analogy Inc., Beaverton, OR, 1992.

[10] Preisach, V. F. (1935)
Überdie magnetische Nachwirkung.
Zeitschrift für Physik, **94** (Mar./May 1935), 277.

[11] Hsu, J. T., and Ngo, K. D. T. (1997)
Finite-element formulation of field-based subcircuits for modeling of magnetic components with hysteresis.
IEEE Transactions on Power Electronics, **12**, 3 (May 1997), 414–421.

[12] Jiles, D. C. (1993)
Frequency dependence of hysteresis curves in non-conducting magnetic materials.
IEEE Transactions on Magnetics, **29**, 6 (Nov. 1993).

[13] Prigozy, S. (1993)
PSpice computer modeling of hysteresis effects.
IEEE Transactions on Education, **36**, 1 (Feb. 1993), 2–5.

[14] Lederer, D. et al. (1999)
On the parameter identification and application of the Jiles–Atherton hysteresis model for numerical modeling of measured characteristics.
IEEE Transactions on Magnetics, **35**, 3 (May 1999), 1211–1214.

[15] Wilson, P. R., Ross, J. N., and Brown, A. D. (2001)
Optimizing the Jiles–Atherton model of hysteresis by a genetic algorithm.
IEEE Transactions on Magnetics, **37**, 2 (Mar. 2001), 989–993.

[16] *Philips Components* (1997)
Philips Magnetic Products, Saugerties, NY, Nov. 1997.

[17] Deane, J. H. B. (1994)
Modeling the dynamics of nonlinear inductor circuits.
IEEE Transactions on Magnetics, **30**, 5 (Sept. 1994), 2795–2801.

[18] Ngo, K. D. T., Srinivas, S., and Nakmahachalasint, P. (2001)
Broadband Extended cantilever model for magnetic component windings.
IEEE Transactions on Power Electronics, **16**, 4 (July 2001), 551–557.

3-D Track Initiation in Clutter Using 2-D Radar Measurements

We present an algorithm for initiating 3-D tracks using range and azimuth (bearing) measurements from a 2-D radar on a moving platform. The work is motivated by the need to track possibly low-flying targets, e.g., cruise missiles, using reports from an aircraft-based surveillance radar. Previous work on this problem considered simple linear motion in a flat Earth coordinate frame [7]. Our research extends this to a more realistic scenario where the Earth's curvature is also considered. The target is assumed to be moving along a great circle at a constant altitude. After the necessary coordinate transformations, the measurements are nonlinear functions of the target state and the observability of target altitude is severely limited. The observability, quantified by the Cramer–Rao lower bound (CRLB), is very sensitive to the sensor-to-target geometry. The paper presents a Maximum Likelihood (ML) estimator for estimating the target motion parameters in the Earth-centered Earth-fixed (ECEF) coordinate frame from 2-D range and angle measurements. In order to handle the possibility of false measurements and missed detections, which was not considered in [7], we use the Probabilistic Data Association (PDA) algorithm to weight the detections in a frame. The PDA-based modified global likelihood is optimized using a numerical search. The accuracies obtained by the resulting ML-PDA estimator are quantified using the CRLB for different sensor-target configurations. It is shown that the proposed estimator is efficient, that is, it meets the CRLB. Of particular interest is the achievable accuracy for estimating the target altitude, which is not observed directly by the 2-D radar, but can be only inferred from the range and bearing observations.

Manusript received July 1, 2001; revised May 3, 2002.

IEEE Log No. T-AES/38/4/06567.

Refereeing of this contribution was handled by X. R. Li.

I. INTRODUCTION

The problem we are studying here is to find an aircraft's altitude, speed, and trajectory in 3-D space from a sequence of (2-D) slant range and bearing reports. The work is motivated by the need to track possibly low-flying targets, e.g., cruise missiles, using reports from an aircraft-based radar.

Previous work on this problem [7] was based on some restrictive assumptions. It assumed that the Earth can be considered flat when the radar range is much smaller than the Earth's radius, and also it assumed that the target is performing rectilinear motion at a given altitude. The work was done in the cylindrical coordinate system centered at the own ship [7]. These assumptions are, however, not reasonable for an aircraft flying at high altitude, where the curved Earth becomes relevant due to the extended horizon. Our research extends this to consider the Earth's curvature, as well as allowing for measurement origin uncertainty.

In our research, the target and the sensor platform are assumed to be moving at a constant speed and altitude along a great circle. Thus the target's motion is characterized by a 5-dimensional parameter vector. After the necessary coordinate transformations, the measurements are nonlinear functions of the target state. The observability of the target parameter vector, quantified by the Cramer–Rao lower bound (CRLB), is very sensitive to the sensor-to-target geometry. A maximum likelihood (ML) estimator is presented for estimating the target motion parameters in the Earth-centered Earth-fixed (ECEF) coordinate frame. In order to handle the possibility of false measurements and missed detections, which was